INTERNATIONAL ATOMIC ENERGY AGENCY
UNITED NATIONS EDUCATIONAL, SCIENTIFIC AND CULTURAL ORGANIZATION

INTERNATIONAL CENTRE FOR THEORETICAL PHYSICS
34100 TRIESTE (ITALY) - P.O.B. 586 - MIRAMARE - STRADA COSTIERA 11 - TELEPHONES: 224281/2/3/4/5/6
CABLE: CENTRATOM - TELEX 460392-I

SMR/115 - 34

WINTER COLLEGE ON LASERS, ATOMIC AND MOLECULAR PHYSICS

(21 January - 22 March 1985)

SEMICONDUCTOR LASERS & PICOSECOND OPTOELECTRONICS

E.O. GOEBEL
Max-Planck-Institut fuer Festkoerperforschung
Heisenbergstrasse, 1
Postfach 80 06 65
7000 Stuttgart 80
Fed. Rep. Germany

SEMICONDUCTOR LASERS & PICOSECOND OPTOELECTRONICS

E.O. GÖBEL

PART I: SEMICONDUCTOR LASERS

PART II: OPTICAL PROPERTIES

PART III: PS-OPTOELECTRONICS

SEMICONDUCTOR LASERS

PART I

FUNDAMENTALS
EXCITATION (HETERODIODE)
LASER STRUCTURE
QUANTUM WELL LASER
TECHNOLOGY
APPLICATIONS

FUNDAMENTALS

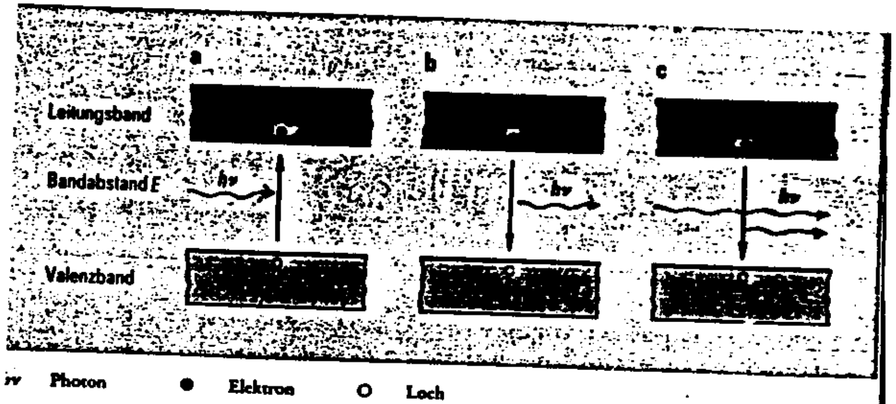

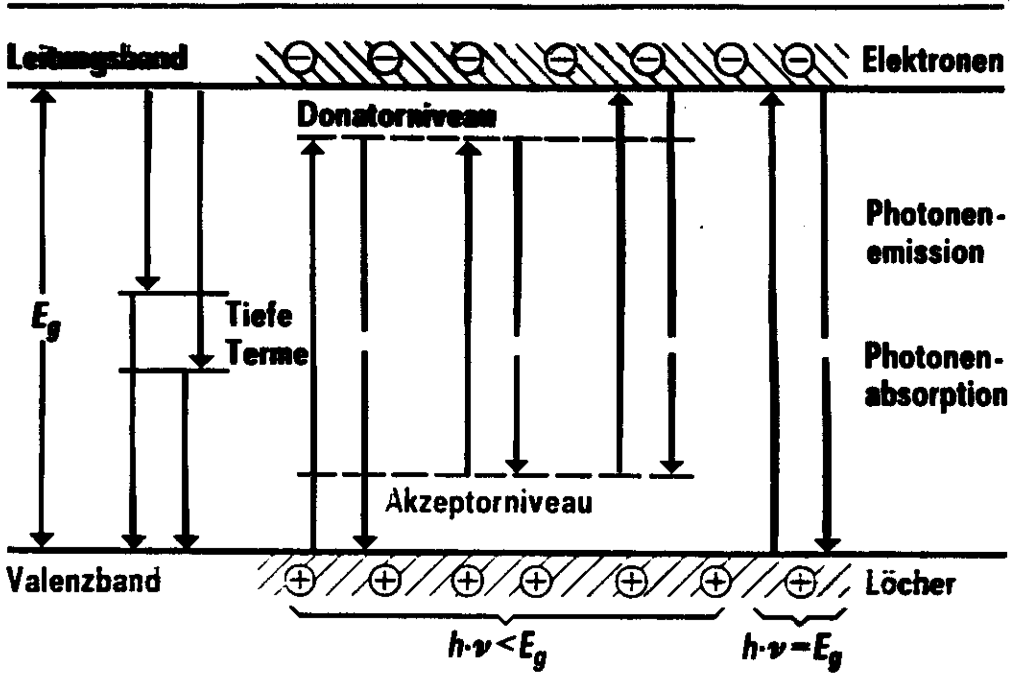

Grenzwellenlänge $\lambda_{grenz} = \frac{h \cdot c}{E_g} \approx \frac{1240}{E_g\,(eV)}$ (nm)

Halbleiter	E_g (300 K)	λ_{grenz}	Bandübergang
Ge	0,7 eV	1800 nm	indirekt
Si	1,1 eV	1100 nm	indirekt
GaAs	1,4 eV	840 nm	direkt
GaP	2,3 eV	560 nm	indirekt
SiC	2,8 eV	440 nm	indirekt
GaN	3,5 eV	350 nm	direkt

h Plancksches Wirkungsquantum
ν Frequenz ($\nu = \frac{c}{\lambda}$)
c Lichtgeschwindigkeit
E_g Energielücke

Bänderschema im Ortsraum und Grenzwellenlängen

bo015/1

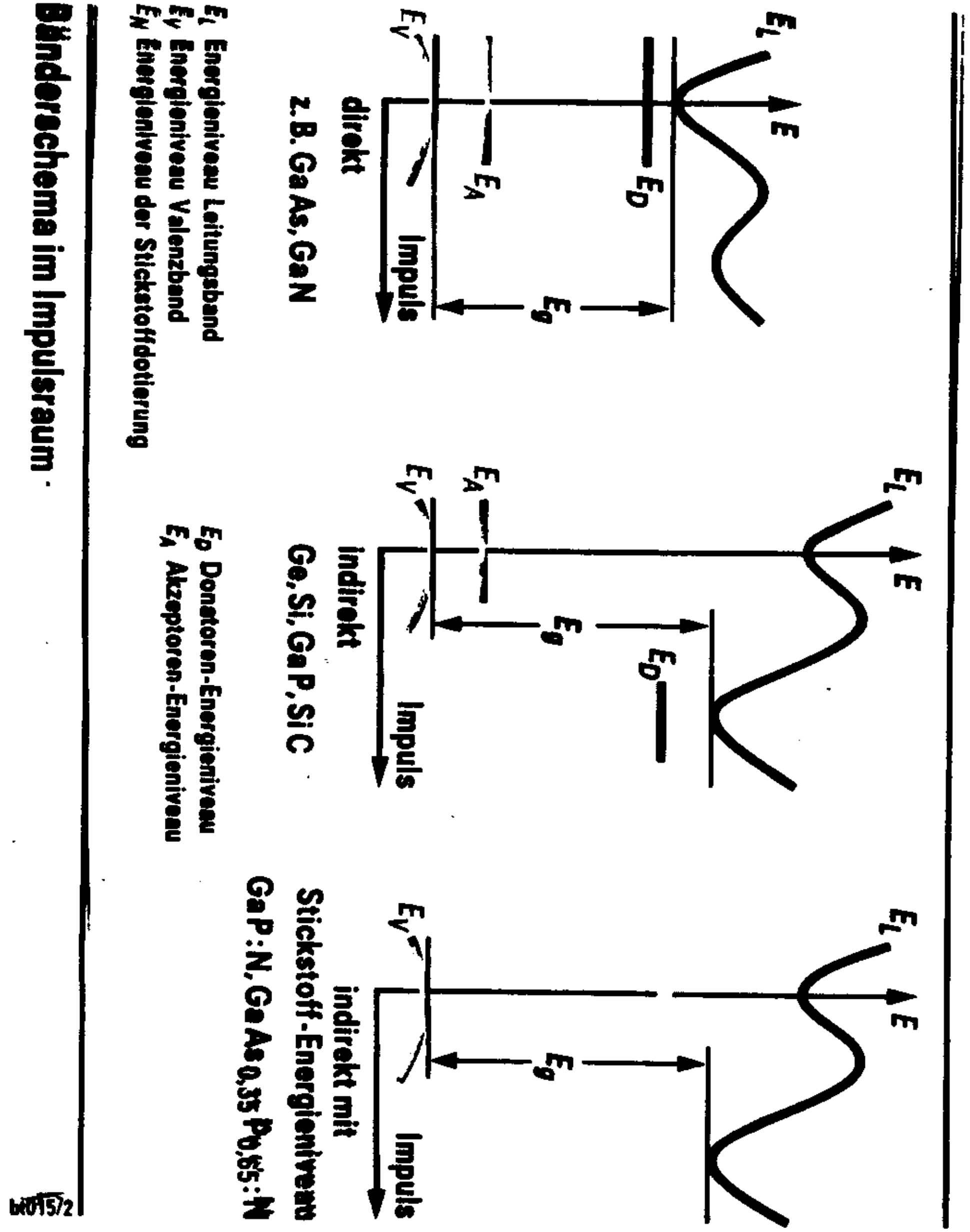

Band - to - Band Optical Transitions

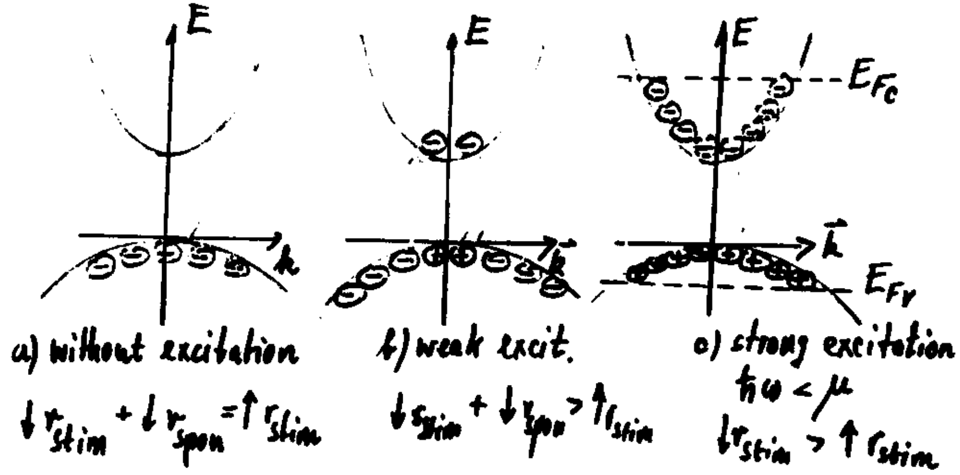

$$f_c(E_c') = \frac{1}{e^{(E_c' - E_{Fc})/kT} + 1}$$

$$f_v(E_v') = \frac{1}{e^{(E_v' - E_{Fv})/kT} + 1}$$

Transition between E_c' and E_v' : $E_c' - E_v' = \hbar\omega$

1.) $r'_{spon} \downarrow$: $r'_{spon}(\hbar\omega) = C_{cv} \cdot f_c(E_c')\,(1 - f_v(E_v'))$

2) $r_{stim}\downarrow$: $\quad r_{stim}(\hbar\omega) = B_{cv}\, f_c\,(1-f_v)\cdot\tilde{N}$

3) $r_{stim}\uparrow$: $\quad r_{stim}(\hbar\omega) = B_{vc}\, f_v\,(1-f_c)\cdot\tilde{N}$

detailed balance (without excitation):

$$r'_{spon}\downarrow + \tilde{N}_0\cdot r_{stim}\downarrow = \tilde{N}_0\, r_{stim}\uparrow$$

$$\Rightarrow \quad C_{cv} = B_{cv} = B_{vc} \equiv B(\hbar\omega)$$

$$r'_{stim}(\hbar\omega) = r_{stim}(\hbar\omega)\downarrow - r_{stim}(\hbar\omega)\uparrow =$$

$$r'_{spon}(\hbar\omega)\left\{1 - e^{(\hbar\omega-(E_{Fc}-E_{Fv}))/kT}\right\}$$

$$\boxed{r'_{stim}(\hbar\omega) > 0 \Leftrightarrow \hbar\omega < \Delta E_F}$$

$$\left(\hat{=}\ N_2 > \frac{g_2\cdot N_1}{g_1}\ \right)$$

<u>total rate:</u>

$$r_{spon}(\hbar\omega) = \sum_{\substack{E'_c \\ E'_c-\hbar\omega = E_v}} r'_{spon}(\hbar\omega)$$

<u>two cases:</u>

1.) only transitions with $\vec{k}_c - \vec{k}_v = \vec{k}_{ph} \simeq 0$
(k-selection rule)

$$r_{spon}(\hbar\omega) = B(\hbar\omega)\cdot\rho_{joint}\, f_c\,(1-f_v)$$

$$r_{stim}(\hbar\omega) = B(\hbar\omega)\cdot\rho_{joint}\,(f_c-f_v)$$

isotropic, parabolic bands:

$$\rho_{joint} = \frac{4\pi}{h^3}\left(2m_j^*\right)^{3/2}\left(\hbar\omega - E_g\right)^{1/2}$$

$$\frac{1}{m_j} = \frac{1}{m_e} + \frac{1}{m_h}$$

2) no k-selection rule

$$r_{spon}(\hbar\omega) = \int B(E'_c)\cdot\rho_c(E'_c)\cdot\rho_v(E'_c-\hbar\omega)\cdot f_c(E'_c)\cdot\left(1-f_v(E'_c-\hbar\omega)\right)\cdot dE'_c$$

$$r_{stim}(\hbar\omega) = \ ...$$

$$\rho = \frac{4\pi}{h^3}\, M^{2/3}\left(2m_d^*\right)^{3/2}\cdot\left(E-E_g\right)^{1/2}$$

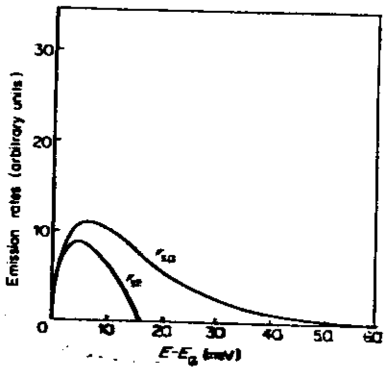

Fig. 2.4. Emission rates with k-selection rule calculated from eqns. (2.120) and (2.121)

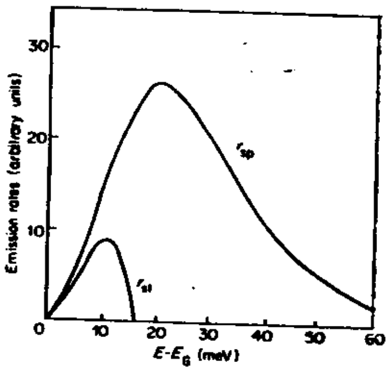

Fig. 2.5. Emission rates without k-selection rule calculated from eqns. (2.122) and (2.123)

1) III-V Compound Semiconductors

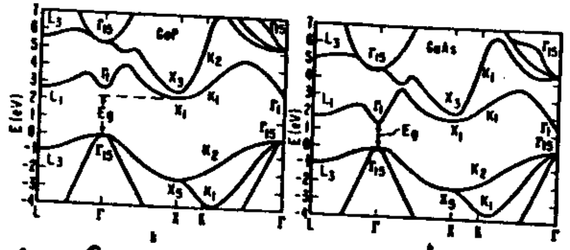

GaAs, GaAlAs, InP, GaInAsP, GaInAs
Valenceband at Γ-point (degenerated)
Conductionband at Γ (L, X)

2.) IV-VI Compound Semiconductors (Lead Salts)

PbS, PbTe, PbSe etc.

4 aequivalent valence- and conduction band extrema at L-point

3.) Quantum Wells (2D free electron and holes)

GaAs/GaAlAs, GaInAsP/InP etc.

EXCITATION

- Optical ($\hbar\omega > E_g$)
- electron beam
- electrical (p-n junction)
  the heterodiode

p-n junction

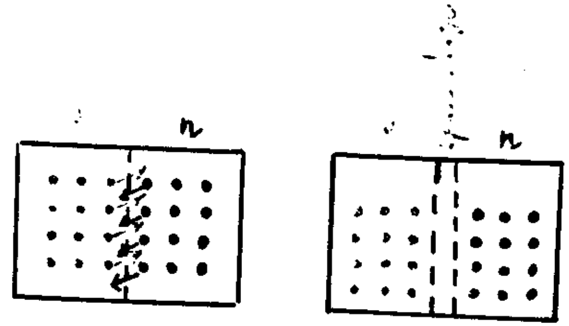

without voltage

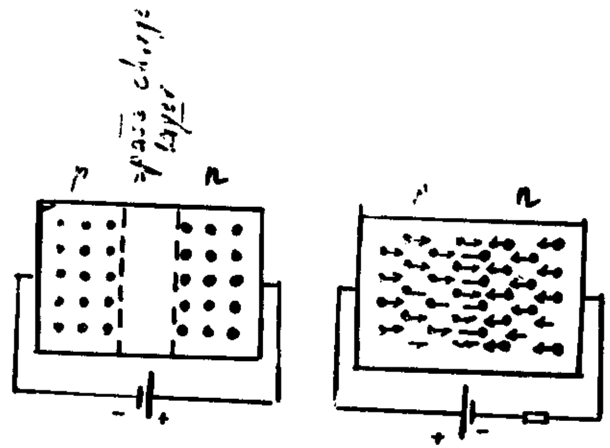

reverse forward

bias

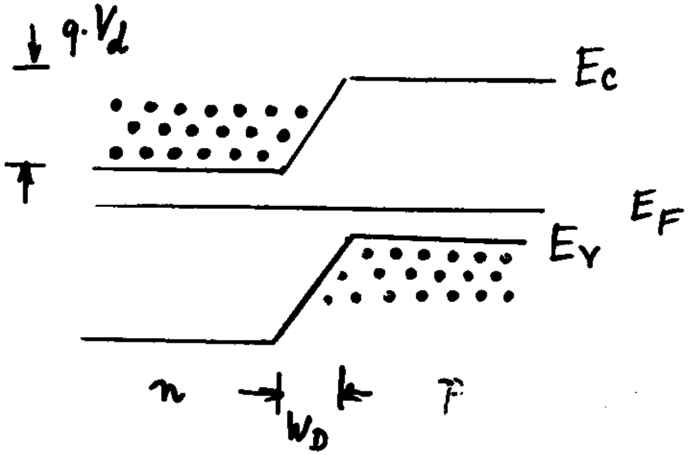

without bias

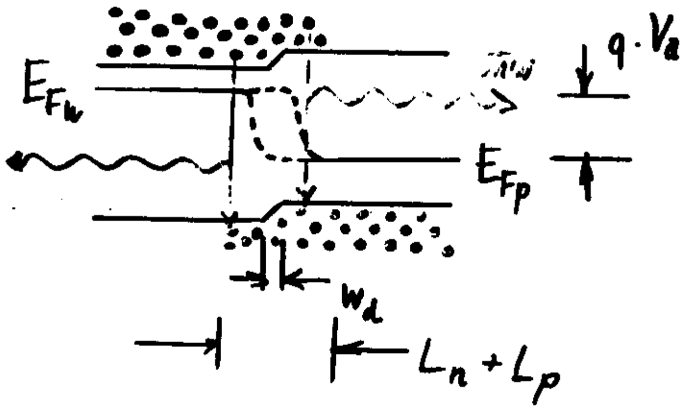

forward bias

I-V Characteristics

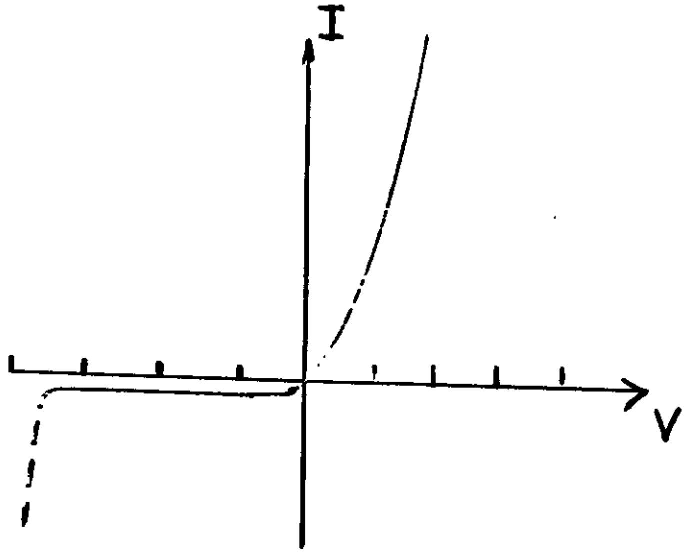

$$I = I_o \left(e^{qV/nkT} - 1 \right)$$

$$1 \leq n \leq 2$$

$n = 1$ Diffusion Current
$n = 2$ Recombination Current

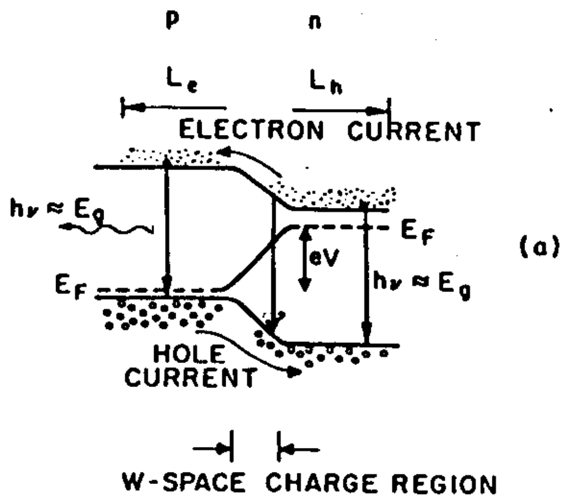
p
n
L_e
L_n
ELECTRON CURRENT
$h\nu \approx E_g$
E_F
eV
E_F
$h\nu \approx E_g$
HOLE CURRENT
W-SPACE CHARGE REGION

(a)

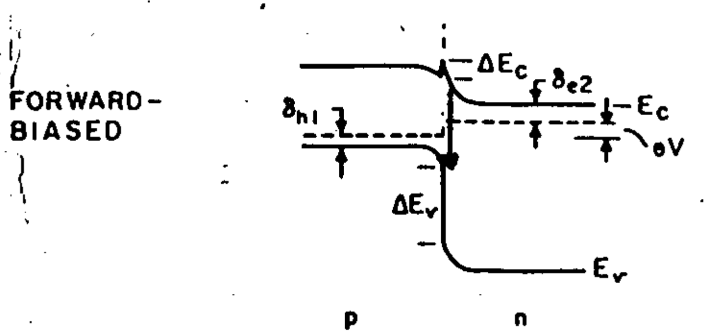
FORWARD-BIASED
ΔE_c
δ_{e2}
E_c
δ_{h1}
eV
ΔE_v
E_v
p
n

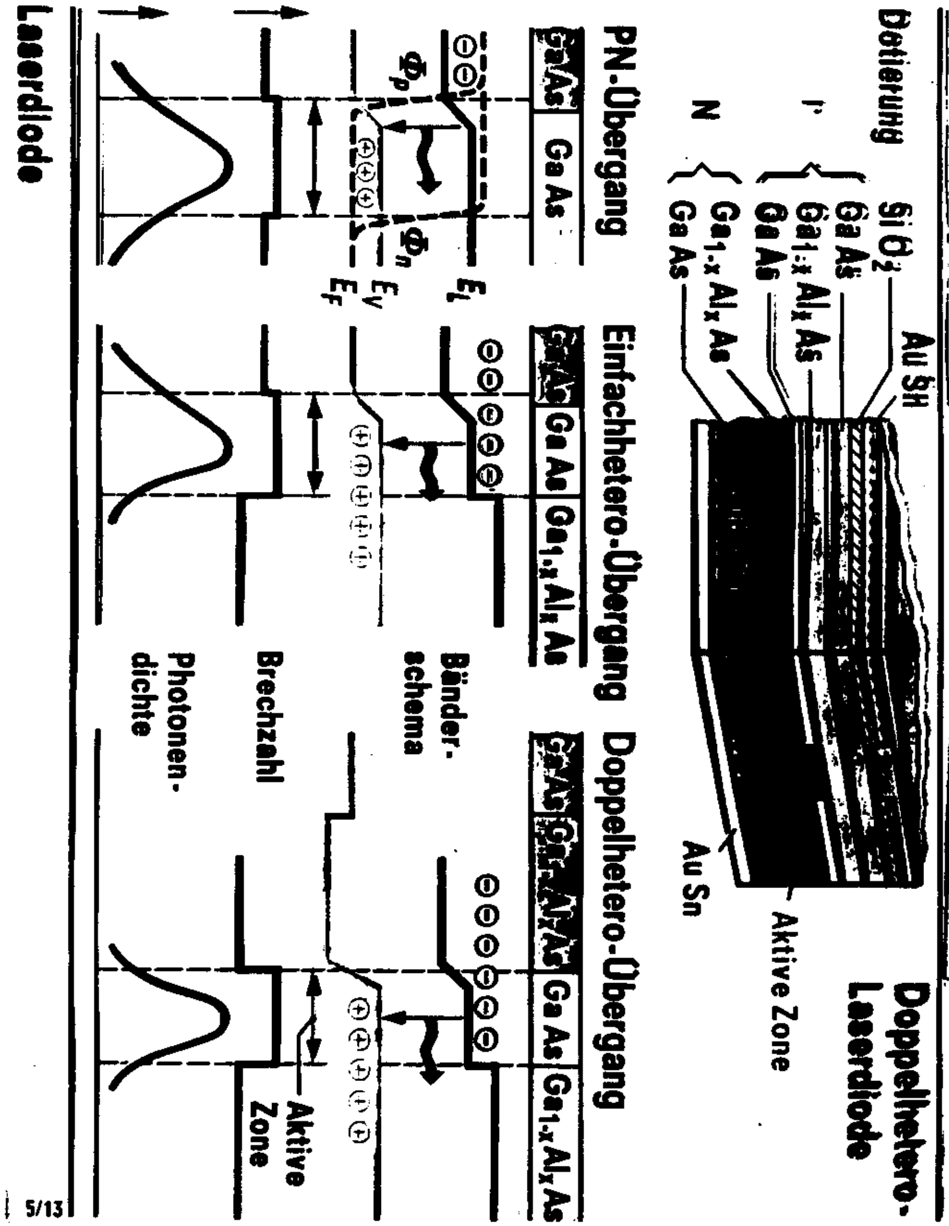
Doppelhetero-Laserdiode
Dotierung
P
N
SiO_2
GaAs
$Ga_{1-x}Al_xAs$
GaAs
$Ga_{1-x}Al_xAs$
GaAs
Au Sn
Au Sn
Aktive Zone
PN-Übergang
Einfachhetero-Übergang
Doppelhetero-Übergang
GaAs
$Ga_{1-x}Al_xAs$
Φ_p
Φ_n
E_L
E_V
E_F
Bänder-schema
Brechzahl
Photonen-dichte
Aktive Zone
Laserdiode
5/13

Requirements for "Hetero-Materials"

1) larger band gap energy
2) lower refractive index
3) same lattice constant

mixed compound semiconductors

- $Al_x Ga_{1-x} As$
- $Ga_x In_{1-x} As_y P_{1-y}$
- $Pb_{1-x} Sn_x Te$

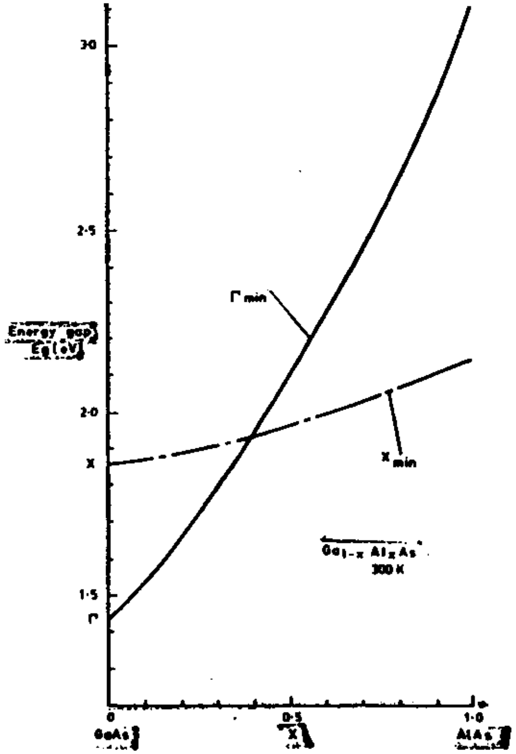

Figure 3.9 The direct and indirect energy gaps of $Ga_{1-x}Al_x$ (after Casey and Panish[21])

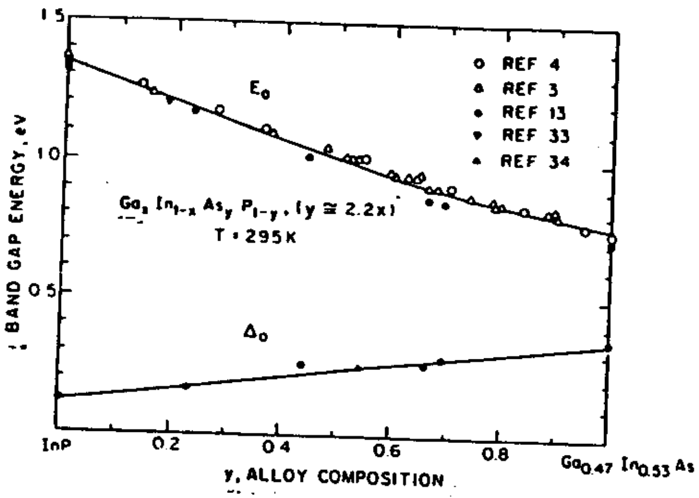

Figure 12.4 The energy gap (E_0) and spin–orbit splitting at the zone centre (Δ_0) in GaInAsP as function of alloy composition at 295 K. The full curves are calculated using the expressions given i the text and the disorder bowing shown in Figure 12.2. The measured data show very little scatter an are in excellent agreement with the theoretical curves

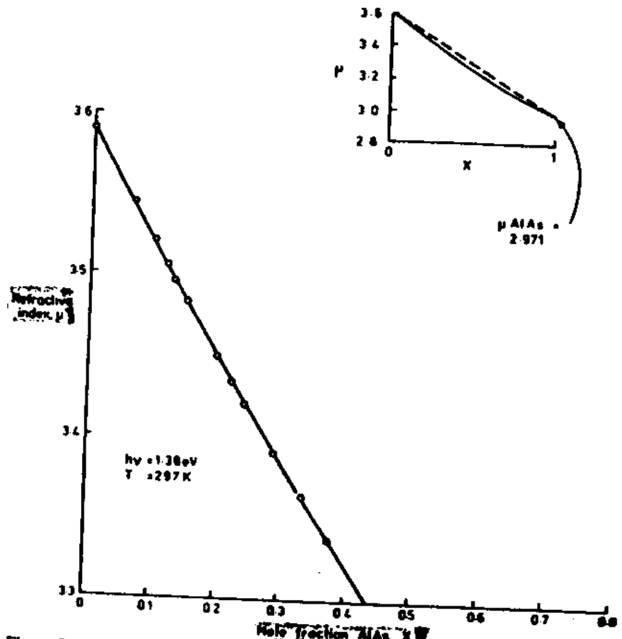

Figure 3.11 Refractive index of n-type $Ga_{1-x}Al_xAs$ at $h\nu$ = 1.38 eV as a function of composition x (after Casey *et al.*[22])

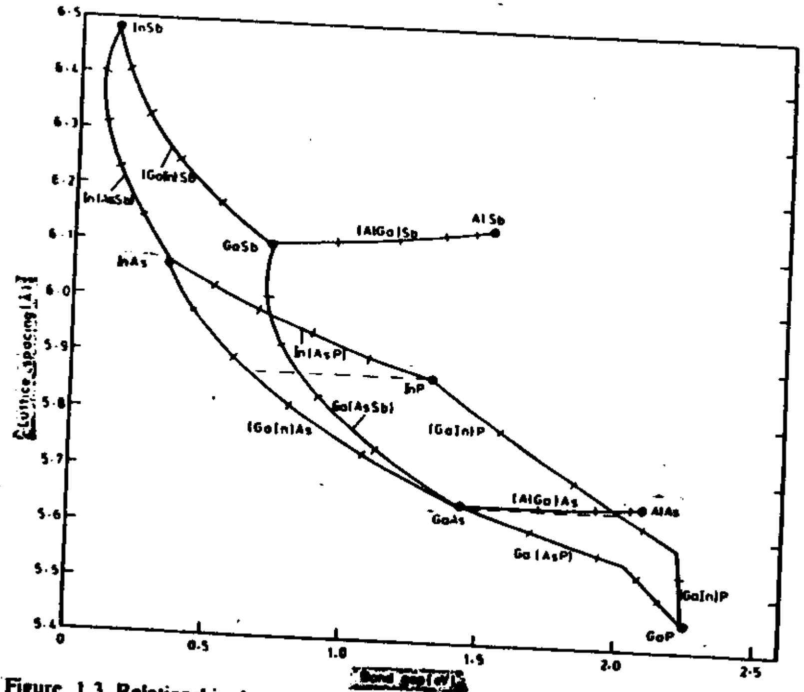

Figure 1.3 Relationship between band gap and lattice spacing in a number of mixed III/V semiconductors containing ternary combinations of Al, Ga, In and P, As, and Sb

substrate materials : GaAs, InP, GaSb

- GaAs/GaAlAs : o.k. ($x < 0.38$)
- InGaAsP/InP : o.k. ($In_{0.53}Ga_{0.47}As$) ($\lambda = 1.7\,\mu m$)

InGaAsSb/GaSb

LASER STRUCTURE

Laser (conventional)

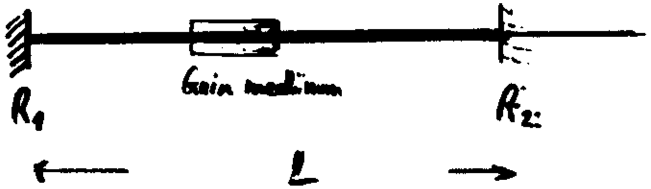

lasing: $R_1 \cdot R_2 \exp 2(g-\alpha)\cdot L \geq 1$

Semiconductor laser:

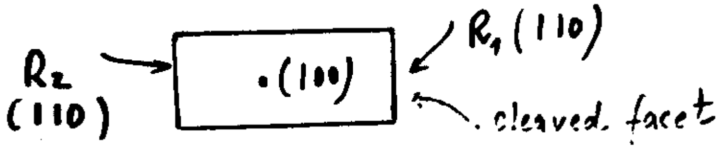

	conv. laser	semicond. laser
R_1	100%	30%
R_2	95%	30%
$(g-\alpha)$	$1 \ldots 10\ cm^{-1}$	$100\ cm^{-1}$
L	1 m	200 µm

Modes:

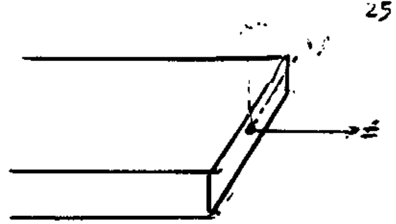

longitudinal modes (z):

$$L = q\,\frac{\lambda}{2n^*(\lambda)} \Rightarrow \Delta\lambda = \frac{\lambda^2}{2L\left(\lambda\frac{dn^*}{d\lambda} - n^*\right)}$$

transversal modes (x,y):

$$\left[\nabla^2 + (n^* k)^2\right]\vec{E} = 0$$

$$n^* = n_1 - i n_2 = n(x,y)$$

Ansatz: $n^{*2}_{(x,y)} = n_0^{*2}\left[1 - \left(\frac{x}{x_0}\right)^2 - \left(\frac{y}{y_0}\right)^2\right]$

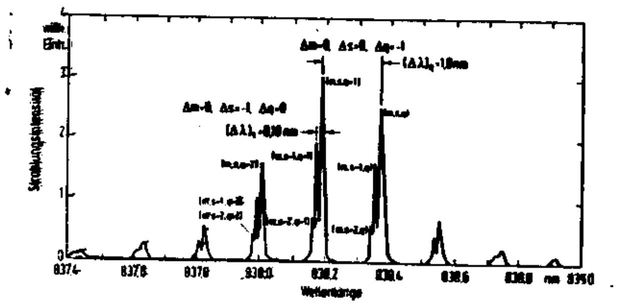

Abb. 8.16. Hochaufgelöstes Emissionsspektrum einer GaAs-Laserdiode. Man erkennt die axialen Grundmoden mit ihrem Abstand von 0,18 nm und ihre Satelliten

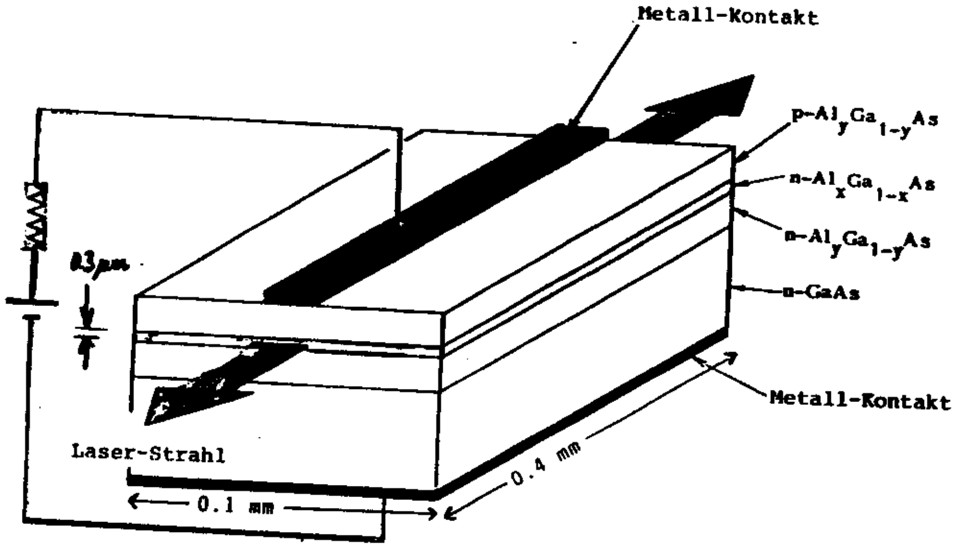

fundamental transverse mode stabilization

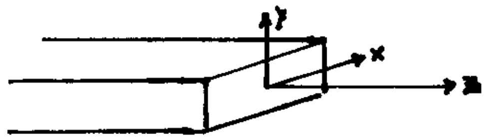

x-direction: no problem (d = 0.3μm)

y-direction: 1. gain guiding (current)

2. index guiding (refr. index)

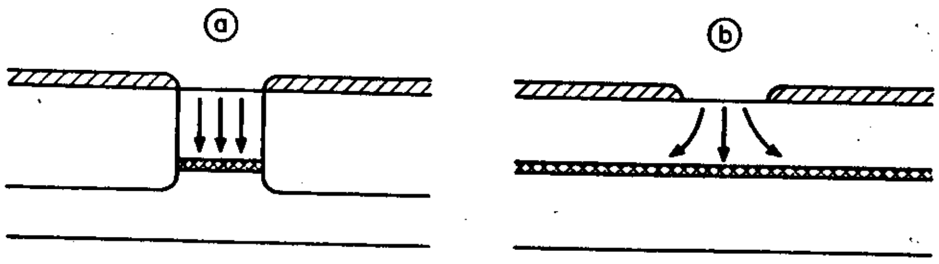

index guiding

gain guiding

buried heterostructure
channeled substrate planar
metal clad ridge waveguide
⋮

oxide stripe
V-groove
proton implanted

ohne laterales Confinement

mit lateralem Confinement

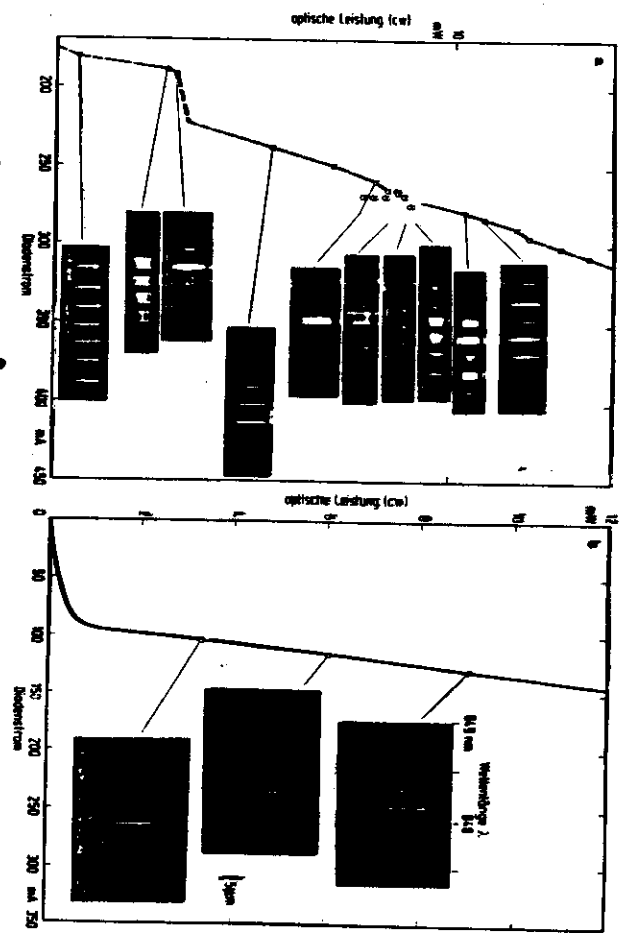

Index-Guided Laser

Burried-**H**eterostructure

BH-
(Hitachi)

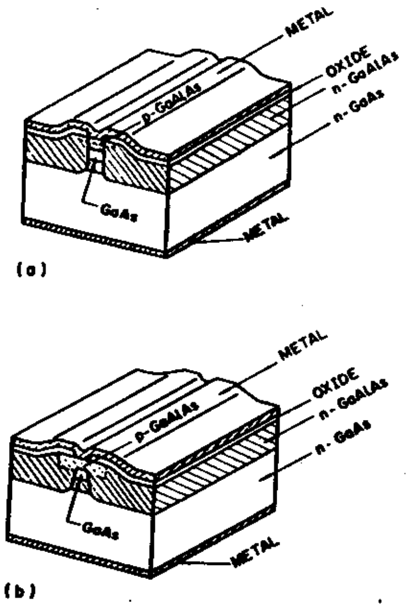

FIG. 1. Buried-heterostructure injection lasers. In both (a) type-I and (b) type-II lasers, the GaAs active regions are completely surrounded by GaAlAs. The lasers are typically 400 μm long, 300 μm wide, and 100 μm thick. The height of the raised area near the stripe region is about 1 μm or less. The drawings are not to scale in order to show the various regions clearly.

Channeled-**S**ubstrate
Planar

CSP-
(Hitachi)

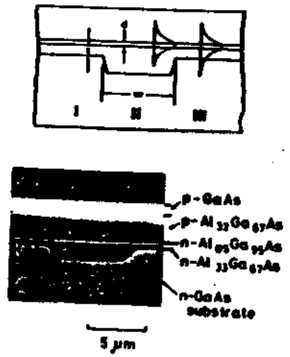

FIG. 1. Cross-sectional view of a channeled-substrate planar (CSP) laser perpendicular to the direction of light propagation (top), and a SEM photograph of the cleaved crystal face (bottom).

Quantum Well Lasers

- tunable band gap
- lower threshold ?
- less temperature sensitivity ?
- better noise performance ?

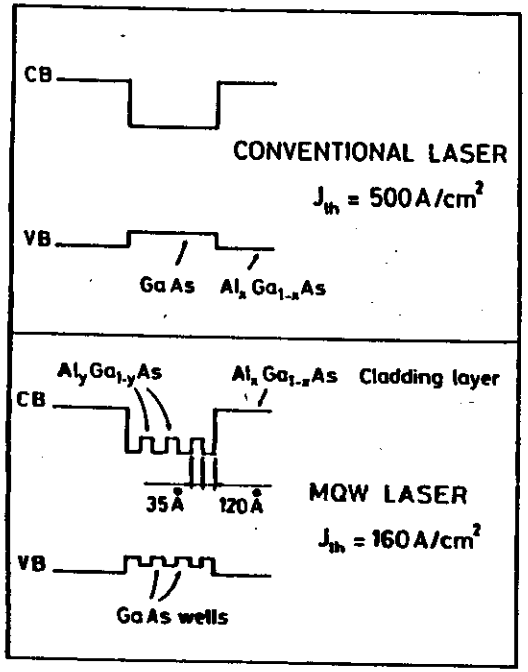

Schematic band diagram of a multiple quantum well laser (after Tsang [31]) with respect to conventional laser. Note the improvement in threshold current in MQW laser.

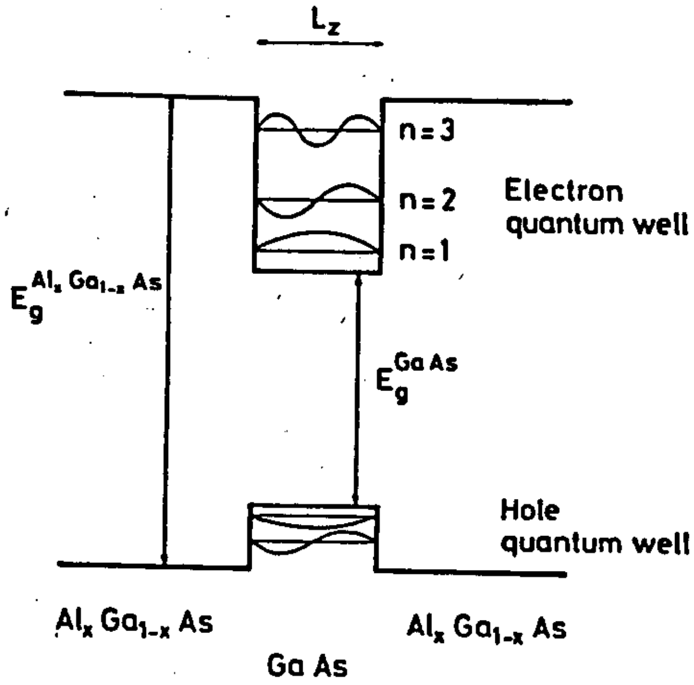

Quantum well in $Al_xGa_{1-x}As/GaAs/Al_xGa_{1-x}As$ double heterojunction: the lattice match between GaAs and $Al_xGa_{1-x}As$ leads to a perfect quantum well

$$E = E_{\parallel} + E_n$$

$$E_n = \frac{\hbar^2}{2m^*}\left(\frac{n \cdot \pi}{L_z}\right)^2$$

$$E_{\parallel} = \frac{\hbar^2}{2m^*}\left(k_x^2 + k_y^2\right)$$

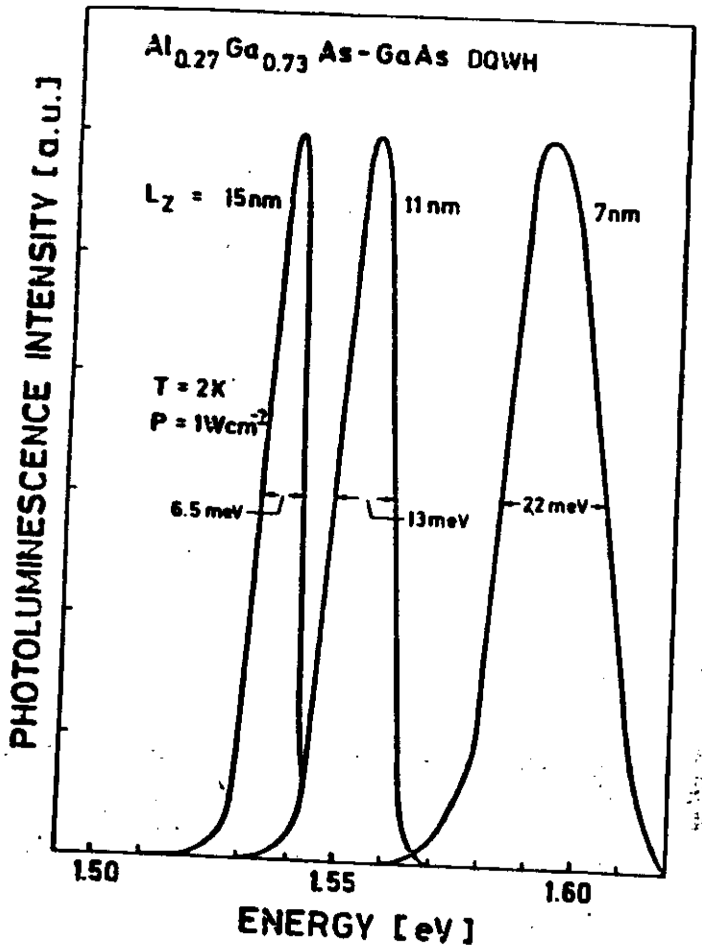

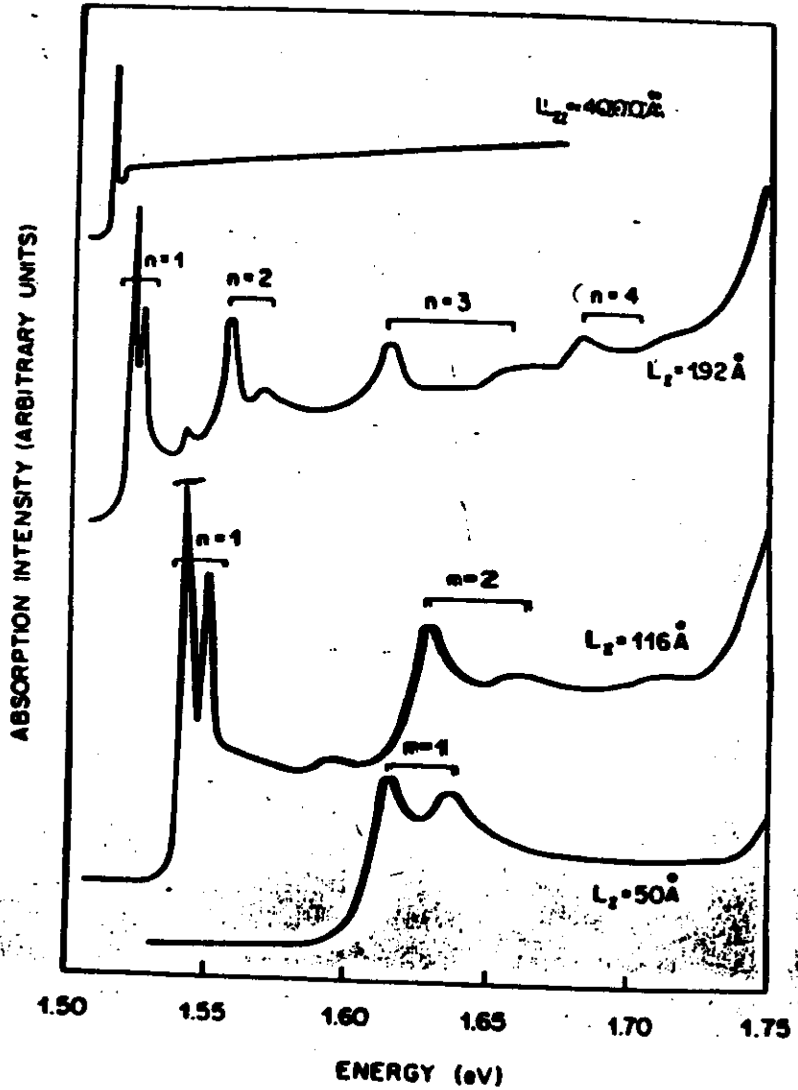

Fig. 7 Shift of photoluminescence of quantum wells with change of well width L_z (after ref. 22,23)

Gossard et al.

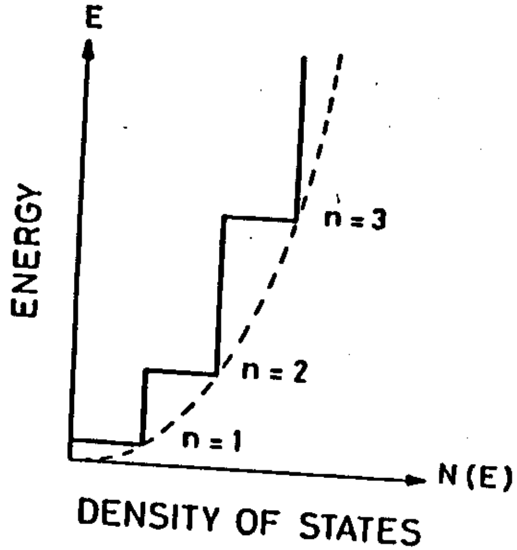

Fig. 7 Step-like density of states in a two-dimensional system

$$\rho(E) = \frac{m^*}{\pi \hbar^2}$$

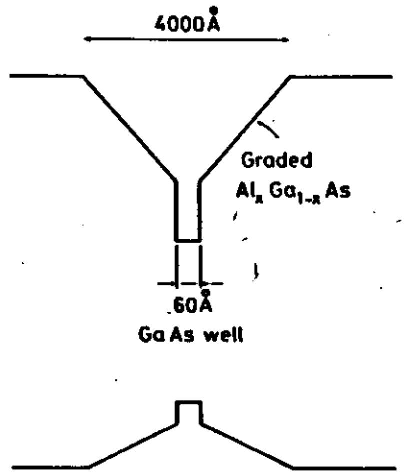

Schematic band diagram of a single-quantum laser positioned in a graded-refractive-index structure (after Hersee et al. [64]). QW lasers of this type present threshold current as low as 121 A/cm^2.

Technology

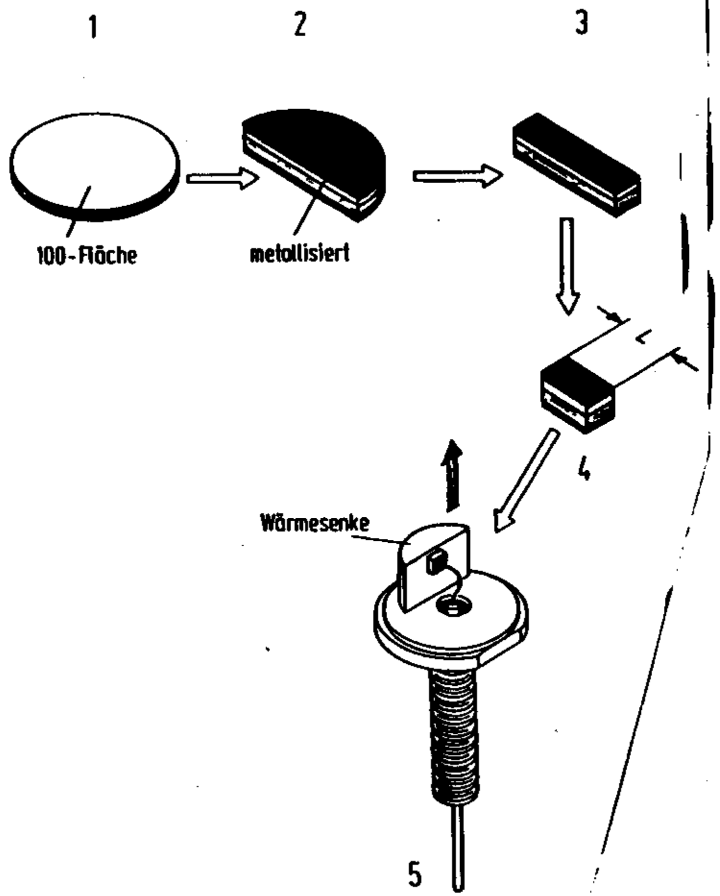

Technologies:

- Liquid Phase Epitaxy (LPE)
- Vapor Phase Epitaxy (VPE)

  Chlorides: $AsCl_3$, PCl_3
  Hydrides: AsH_3, PH_3

- Metal Organic Vapor Phase Epitaxy (MOCVD)

  $Ga(CH_3)_3$, $In(C_2H_5)_3$ } III.

  AsH_3, PH_3 } V.

- Molekular Beam Epitaxy (MBE)

Applications:

- Data Storage (Optical Digital Audio Disc)
  GaAs, GaAlAs (visible lasers)

- Optical Communication (fibres)
  short distance (buildings, cars, plans, ships, nuclear plants)
  GaAs/GaAlAs (850nm)

  long distance, high bit rates: InGaAsP (1.3μm), InGaAs (1.5μm)

- Spektroscopy (IR) lead salt lasers
  2μm — 40μm